American Mineralogist, Volume 88, pages 365–376, 2003

Experimental study of zircon coarsening in quartzite $\pm H_2O$ at 1.0 GPa and 1000 °C, with implications for geochronological studies of high-grade metamorphism

JOHN C. AYERS,* KATHERINE DELACRUZ, CALVIN MILLER, AND ORAN SWITZER

Department of Geology, Vanderbilt University, VU Station B no. 350105, 2301 Vanderbilt Place, Nashville, Tennessee 37235-0105, U.S.A.

ABSTRACT

The rate and mechanism of zircon coarsening in quartzite $\pm H_2O$ at 1.0 GPa and 1000 °C were characterized by performing time-series experiments in a piston-cylinder apparatus. Anhydrous experiments show no significant growth of zircon or textural modifications after 24 h. In the presence of 1–2 wt% H_2O, zircon (2 wt%) in coarsely powdered quartz recrystallized in the first 8 hours so that mean crystal size decreased relative to the starting material. After 8 h zircon grew by Ostwald ripening and by coalescence of crystals, and maintained its position on quartz grain boundaries, even while quartz crystals coarsened, by recrystallizing in the fluid. Fitting the experimental data produced the growth-rate equation $\log (\langle D\rangle^n - \langle D_0\rangle^n) = \log (\langle D\rangle^2 - \langle D_0\rangle^2) = \log (t - t_0) + \log K_n = \log (t - t_0) - 5.9$, where $\langle D\rangle$ is mean diameter in micrometers, the subscript 0 denotes initial value at time zero, t is experiment duration in seconds, and K_n is the growth-rate constant with units of $\mu m^2/s$ (five experiments, $r^2 = 0.988$). A value of $n = 2$ suggests that growth is interface controlled, with the rate limited by dissolution and precipitation on the crystal surface. An equivalent growth-rate equation is $\langle D\rangle - \langle D_0\rangle = K_{1/n}\, t^{1/n} = K_n^{1/n}\, t^{1/n} = (1.12 \times 10^{-3}\ \mu m/s^{1/2})\, t^{1/2}$, a parabolic rate law equation that can be used to demonstrate that zircon in the presence of H_2O at 1000 °C grows fast enough by Ostwald ripening to produce micrometer-thick overgrowths in <10 y. Rapid coarsening of zircon by Ostwald ripening will occur during thermal metamorphism when fluid is present. Addition of fluid (and possibly melt) greatly increases the rate of coarsening, suggesting that most metamorphic rims form nearly instantaneously during fluid influx (or anatexis), and that U-Pb rim ages date such events.

INTRODUCTION

Zircon is the most commonly used mineral for high-temperature geochronometry because it is widespread, crystallizes from magmas and is stable over wide ranges of metamorphic grade, and is resistant to loss of radiogenic Pb, with a closure temperature exceeding 900 °C for most reasonable cooling rates (Cherniak and Watson 2000). In-situ U-Pb dating of zircon using the ion microprobe is now common (e.g., Ayers et al. 2002; Miller et al. 2000; Vavra et al. 1996), and methods are being developed for accurate and precise measurement of U-Pb ages using laser-ablation ICPMS (Horn et al. 2000; Machado and Gauthier 1996) and the electron microprobe (Geisler and Schleicher 2000). Cathodoluminescence and back-scattered electron imaging commonly reveal multiple growth zones within single crystals (Hanchar and Miller 1993) (Fig. 1), and in-situ dating shows that these zones may have grown at distinctly different times and represent discrete events that grossly correlate with tectonic episodes (Miller et al. 2000).

In many situations, a lack of understanding of what causes growth of zircon impedes interpretation of growth ages. Metamorphic zircon growth is generally assumed to occur at peak metamorphic conditions (i.e., peak temperature). However, recent studies have documented growth that occurred over a range of conditions in a single rock suite. For example, zircon crystals in the Ivrea Zone grew during prograde metamorphism in the upper amphibolite facies, and during peak metamorphism in the granulite facies (Vavra et al. 1999). In-situ U-Pb analysis also allowed identification of two distinct younger events involving alteration and Pb loss. Liati and Gebauer (1999) were able to resolve the ages of multiple zircon growth events in a single tectono-metamorphic cycle in rocks from central Rhodope, northern Greece. SHRIMP ages from five different rock types from the HP-HT terrane ranged from 45.3 ± 0.9 to 36.1 ± 1.2 Ma. Clearly, it is not always safe to assume that zircon grows only during peak metamorphism, although in most cases, new growth occurs only during high-grade metamorphism in upper amphibolite, granulite and eclogite facies.

Zircon may be produced by breakdown of Zr-bearing minerals during prograde, peak, or retrograde metamorphism. However, protolithic zircons generally contain most or all of the Zr in most rocks (Roberts and Finger 1997); the only other common minerals known to have significant Zr concentrations are garnet, hornblende, and clinopyroxene (Fraser et al. 1997; Sorensen and Grossman 1989). Garnet and clinopyroxene usually break down only during retrograde metamorphism, which cannot explain the commonly observed prograde and peak metamorphic growth of zircon. Hornblende may break down to form pyroxene + zircon during prograde metamorphism of mafic rocks at very high grade. Except for rocks with abundant hornblende in their protoliths, in closed systems, zircon may only grow by coarsening during prograde and peak metamor-

* E-mail: john.c.ayers@vanderbilt.edu

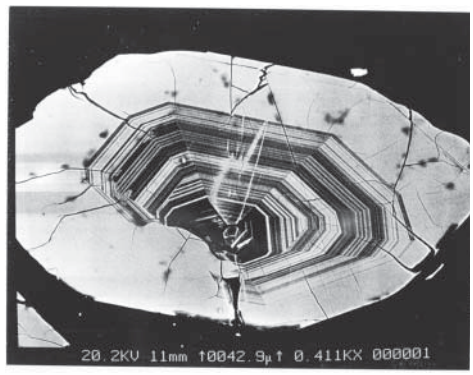

FIGURE 1. Back-scattered electron (BSE) image of natural zircon crystal from heavy mineral sands, Cleveland Co., North Carolina. The igneous core displaying oscillatory zoning was partially resorbed (embayment in lower left corner) before growth of nebulously zoned metamorphic rim (see text). Alternatively, the embayment may mark the previous location of another mineral grain that the zircon crystal had begun to grow around during igneous crystallization and that was subsequently replaced.

phism. For example, in quartzites that contain no other Zr-bearing minerals, and in the absence of open-system transport of Zr, the mass of zircon must be roughly constant during prograde metamorphism, and coarsening is the only possible growth mechanism. The same applies more widely in granitic rocks. Thus, zircon is the only significant source of Zr in many rock types, and zircon crystals in these rocks may only grow through coarsening at the expense of smaller zircon crystals.

The growth of large crystals at the expense of smaller crystals of a dispersed (accessory) mineral is Ostwald ripening, and its driving force is the minimization of surface free energy (Joesten 1991). Ostwald ripening decreases surface free energy by growing large crystals that tend to be nearly spherical (sometimes modified by crystal faces with high Miller indices) because the sphere has the lowest surface area/volume ratio of any shape. As stated by Lasaga (1998), "Ostwald ripening is certainly occurring throughout the earth. In some cases, it may be the dominant mechanism for the exchange of isotopes between solutions and solids, especially where diffusion in the solid is slow." Ostwald ripening will be most important when there is a large range of grain size and when overall grain size is low.

We have observed zircon crystals with thick, unzoned, or nebulously zoned rims that we interpret to be metamorphic, surrounding older igneous cores displaying concentric euhedral or oscillatory zoning, generally in rocks with no other source for Zr other than preexisting zircon (Fig. 1). Overgrowths of this type are common in high-grade metamorphic rocks (Miller et al. 1998), and are the expected product of Ostwald ripening. Overgrowths formed during granulite facies metamorphism are typically nearly spherical, transparent, and unzoned or nebulously zoned (Pidgeon et al. 2000). In this paper, we refer to overgrowths with some or all of these characteristics as "metamorphic rims" or just "rims," recognizing that overgrowths without all of these characteristics may have formed by other growth mechanisms.

Based upon both theory and observations, we infer that preexisting zircon crystals coarsen during metamorphism through Ostwald ripening, and that given sufficient time at high enough grade, only large zircon crystals with relict cores of preexisting material overgrown by metamorphic rims should remain. Several studies have provided evidence of metamorphic coarsening of accessory minerals including zircon. Reconnaissance investigations of textures by Kingsbury et al. (1993) suggested that with increasing metamorphic grade, monazite mean crystal size increases, and Crystal Size Frequency Histograms (CSFH) show a subtle shift from lognormal to normal distributions. This finding is consistent with the observations and predictions of Cashman and Ferry (1988) that initial nucleation produces a lognormal distribution (as observed in contact metamorphic rocks), and subsequent coarsening by Ostwald ripening removes the small crystals and changes the CSFH to normal (as observed in rocks that experienced prolonged regional metamorphism). Recently, Rubatto et al. (2001) observed that zircon and monazite crystal size increased with increasing metamorphic grade. Furthermore, zircon crystals grew only at granulite grade and at the expense of preexisting detrital crystals during anatexis. Likewise, Vavra et al. (1999) documented that the extent of zircon growth increased with metamorphic grade in the upper amphibolite to granulite facies, again associated with anatexis, and suggested that growth occurred via Ostwald ripening. Thus, there is evidence that some accessory minerals used in geochronometry such as zircon and monazite grow by Ostwald ripening during high-grade metamorphism.

Our goal in this study was to characterize the process of zircon growth by Ostwald ripening by annealing zircon crystals in a coarsely crystalline matrix of quartz ±1 wt% H_2O in a piston-cylinder apparatus at 1000 °C and 1.0 GPa. We designed the experiments so that coarsening would be the only possible growth mechanism. Performing a series of experiments of varying duration and measuring the CSFH of zircon in the run products allowed us to characterize the rate and mechanism of Ostwald ripening of zircon.

EXPERIMENTAL PROCEDURES

Methods used are very similar to those described in detail by Ayers et al. (1999).

Starting materials

Optically clear quartz was coarsely crushed in a mortar and pestle to produce powder with a mean Feret diameter (diameter of a circle with the same area as the two-dimensional object) $\langle D \rangle = 3.1 \pm 0.4$ μm (95% confidence limits) with a variance of 23.1 μm^2 (Ayers et al. 1999). To one portion of this powder we added 2 wt% reagent grade ZrO_2 to create the "oxide" starting material. To another portion we added 2 wt% of natural zircon (from Goias, Brazil, Smithsonian NMNH 142834) that was ground until most crystals were <2 μm in diameter to produce the "silicate" starting material. Measurement of zircon crystal diameter in a polished epoxy mount of the silicate starting material (see "Image Analysis Methods") yielded $\langle D \rangle = 0.53 \pm 0.05$ μm with variance = 1.2 μm^2 ("ZG SM" in Table 1). The CSFH of zircon is lognormal (Fig. 2a), similar to what it would be at the completion of nucleation and the onset of coarsening

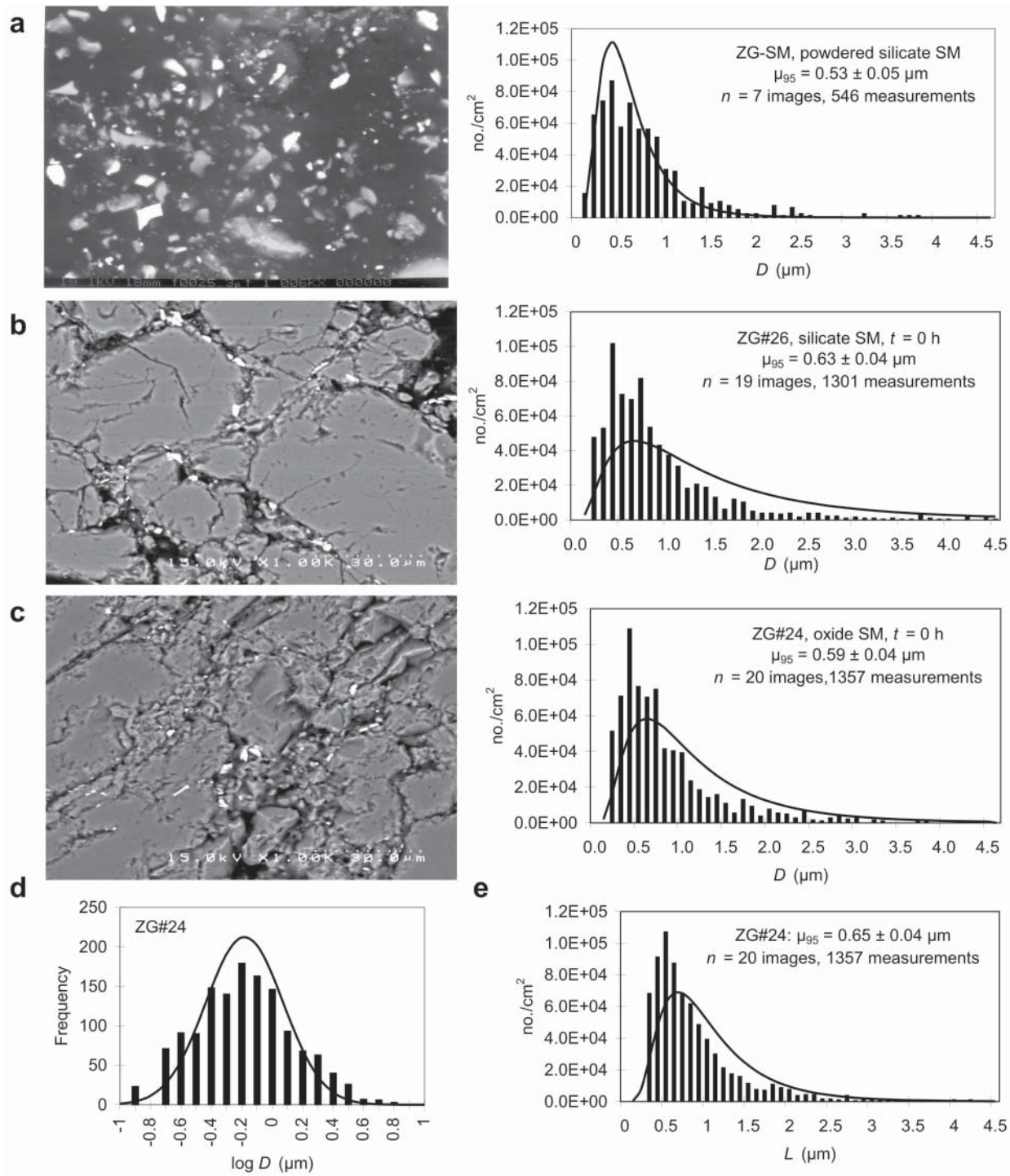

FIGURE 2. BSE images and Crystal Size Frequency Histograms (CSFH) of zircon in: (**a**) silicate (zircon-bearing) starting material ZG-SM, (**b**) zero-time experiment with silicate starting material ZG no. 26, and (**c**) zero-time experiment with oxide starting material ZG no. 24. In these and all subsequent BSE images zircons are bright white, quartz is grey, and pores and cracks are black. In CSFH, the solid curve is a theoretical lognormal distribution with the same mean and standard deviation as the sample. (**d**) Histogram of log D values in ZG no. 24. The solid curve is a theoretical normal distribution with the same mean and standard deviation as the sample. (**e**) CSFH of mean intercept length *L* for ZG no. 24.

TABLE 1. Experimental conditions and measured zircon crystal size parameters

Expt.	Composition*	*t* (h)	no. images	n	Avg. Mag.	Area (μm²)	N_A (μm^{-2})	$A_A = V_V$%	<D> (μm)†	95% CL‡	Variance
ZG SM	Q + 2% Z	0	7	546	819	9.88E + 04	5.52E-03		0.53	0.05	0.30
ZG no. 5	Q + 2% ZrO_2 + 1% H_2O	70	8	364	1000	7.58E + 04	4.80E-03		1.02	0.05	0.54
ZG no. 6	Q + 2% ZrO_2 + 1% H_2O	22.2	5	139	1000	4.74E + 04	2.94E-03		1.43	0.08	0.85
ZG no. 9	Q + 2% ZrO_2	24	*No zircon in run products								
ZG no. 10	Q + 2% ZrO_2 + 1% H_2O	167	4	1008	1010	3.71E + 04	2.71E-02		0.93	0.03	0.29
ZG no. 12	Q + 2% Z + 1% H_2O	8	7	786	754	1.17E + 05	6.72E-03		0.37	0.02	0.13
ZG no. 13	Q + 2% ZrO_2 + 1% H_2O	8	20	1556	1000	1.89E + 05	8.23E-03	0.50	0.63	0.02	0.19
ZG no. 14	Q + 2% Z + 1% H_2O	22	7	582	549	2.20E + 05	2.65E-03		0.44	0.03	0.14
ZG no. 15	Q + 2% Z + 1% H_2O	72	9	933	540	2.92E + 05	3.20E-03		0.54	0.03	0.24
ZG no. 18	Q + 2% Z + 1% H_2O	133.4	20	1305	1000	1.89E + 05	6.89E-03	1.46	0.80	0.03	1.23
ZG no. 19-2	Q + 2% Z	24	17	3933	1000	1.56E + 05	2.53E-02	0.93	0.48	0.01	0.13
ZG no. 20-2	Q + 2% ZrO_2 + 2% H_2O	336	20	1292	1000	1.89E + 05	6.84E-03	1.63	1.20	0.04	0.65
ZG no. 21	Q + 2% Z + 1% H_2O	72	20	1073	1000	1.89E + 05	5.67E-03	2.04	1.17	0.08	1.79
ZG no. 22-2	Q + 2% ZrO_2 + 1% H_2O	87.5	20	1894	1000	1.83E + 05	1.03E-02	1.26	0.77	0.03	0.54
ZG no. 23	Q + 2% ZrO_2 + 1% H_2O	22.2	20	2076	1000	1.83E + 05	1.13E-02	0.48	0.52	0.02	0.14
ZG no. 24	Q + 2% ZrO_2 + 1% H_2O	0	20	1357	1000	1.83E + 05	7.41E-03	0.68	0.59	0.04	0.46
ZG no. 25	Q + 2% ZrO_2 + 1% H_2O	167	25	2298	1000	2.29E + 05	1.00E-02	1.43	0.89	0.03	0.54
ZG no. 26	Q + 2% Z + 1% H_2O	0	19	1301	1000	1.74E + 05	7.48E-03	0.82	0.63	0.04	0.62
ZG no. 27	Q + 2% Z	1	20	1302	1000	1.83E + 05	7.11E-03	0.78	0.66	0.04	0.58

* Z = zircon. All experiments at 1000 °C and 1.0 GPa. All starting materials contain 98% coarsely crushed quartz powder.
† Because measured values of Feret diameter D and mean intercept length L are log-normally distributed except in the upper and lower tails, we calculated a 95% trimmed mean of the $\log_{10}$ transformed values and took the antilog to obtain our best estimate of the population means <*D*> and <*L*>.
‡ 95% confidence limit on estimate of mean value of D, e.g., for ZG no. 27 there is a 95% probability that the population (true) mean falls within the range 0.66 ± 0.04 μm.
§ L3 is the global mean intercept length (Russ 1990).
|| Shape Factor measures how circular an object is: a circle has a value of 1.0 and a line a value approaching zero.

during progressive metamorphism. X-ray diffraction (XRD) of acetone smears confirmed quartz + baddeleyite in the oxide and quartz + zircon in the silicate starting material, indicating that even after extensive grinding the zircon was crystalline.

Piston-cylinder experiments

Cold-sealing capsules of the type described by Ayers et al. (1992) were used to encapsulate samples. We fired a Ni capsule (I.D. = 4.4 mm, O.D. = 6.35 mm, length = 9–10 mm) in air for 12 h at 1000 °C to form a surface layer of NiO that prevented Ni-Pt interdiffusion, and then tapped in a Pt insert (O.D. = 4.4 mm, tri-crimped and welded shut on one end).

After weighing the capsule, we added ~100 mg of powdered starting material, re-weighed the filled capsule to find the weight of starting material, and then added 1–2 wt% H_2O with a microsyringe. We estimate that each sample placed in a capsule contained more than 1 billion zircon crystals. Sampling statistics suggest that samples taken from our starting material should be unbiased and therefore representative. A Pt lid topped by a Ni lid was placed on top and cold-sealed to the capsule by pressurizing in a 1.91 cm piston-cylinder apparatus. We conducted all experiments using the assembly and corresponding pressure calibration described by Ayers et al. (1992). A WRe_3/WRe_{25} thermocouple and temperature controller maintained *T* within ±5 °C of the setpoint, while we manually maintained *P* within ±500 bars. The thermocouple was calibrated by its manufacturer (Engelhardt) and is accurate to ±1.5 °C. Table 1 lists all experiment conditions.

Upon completion of each experiment, we sectioned the capsule lengthwise to maximize observable surface area, mounted the sections in and impregnated their surfaces with epoxy, and polished the mounts to 0.06 μm. Energy dispersive analysis, XRD of ZG no. 5 run products, and identification in optical grain mounts of selected samples showed that zircon and quartz were the only minerals present in our run products.[1]

Imaging and image-analysis methods

We measured the dimensions of zircon crystals from digitized back-scattered electron (BSE) images using image analysis software. First, we coated sample mounts with a carbon film and then imaged them in back-scattered electron mode with a scanning electron microscope. For ZG no. 2–ZG no. 15 we used an ETEC scanning electron microscope with an accelerating potential of 20 keV, and converted Polaroid photos to digital format using a scanner. ZG no. 18–ZG no. 27 run products were imaged on a Hitachi S-4200 at 1000× magnification and an accelerating voltage of 15 keV (Table 1). Traverses made along the length of each capsule revealed no systematic change in zircon size or modal abundance.

Crystal size was measured from 300 dpi, 256 grey-scale level, 3.5 × 4 in digital back-scattered electron images using computer-automated image analysis (details of methods described in Ayers et al. 1999). The spatial resolution was ~0.11 μm at 1000×, allowing us to detect differences in mean crystal diameter as low as 0.35 μm at the 95% level. We applied a median filter to reduce electronic noise without affecting the size of features, and then calibrated the spatial scale using a scalebar in the image. To measure zircon crystal size we thresholded (segmented) the image by classifying as zircon each pixel with grayscale level greater than a specified threshold value. Zircon crystals that were touching were "separated" by drawing a line between them before making measurements. For every crystal, we measured area, perimeter, Feret diameter, and maximum and minimum diameters. For ZG no. 18–

[1]With the exception of rare unreacted "clots" of ZrO_2 in experiments that used oxide starting material (see "Results").

TABLE 1.—*extended*

<L> (μm)†	L3(μm)§	Shape factor‖
0.58		0.86
1.08	0.60	0.85
1.52	0.80	0.83
1.00	0.48	0.84
0.42	0.35	0.90
0.67	0.34	0.82
0.50	0.38	0.90
0.61	0.66	0.91
0.87	0.72	0.90
0.53	0.29	0.93
1.25	0.70	0.79
1.24	0.95	0.82
0.79	0.46	0.83
0.59	0.31	0.88
0.65	0.55	0.88
0.95	0.59	0.95
0.69	0.54	0.90
0.71	0.51	0.82

ZG no. 27, we made measurements using the *Image Processing Toolkit* (plug-in tools for *Adobe Photoshop* published by Reindeer Software), and for ZG no. 2–ZG no. 15 SPSS SigmaScan Pro.

Histograms of zircon crystal size in starting materials (Fig. 2) and run products (Figs. 3, 4, and 5) have lognormal distributions, so histograms of log D are normally distributed (Fig. 2d). Because parametric statistics require normally distributed data, the antilog of the mean value of log D (the geometric mean) provides the best estimate of the population mean of D. However, the log D distribution deviates significantly from a normal distribution in the upper and lower tails of the distribution, where we made the smallest number of measurements and errors are greatest. Thus, we obtained the most robust estimate of population mean by calculating the 95% trimmed mean of log D by deleting the extreme values in the uppermost and lowermost 5% of the distribution, calculating the mean of log D, and taking the antilog. Table 1 lists mean values of D obtained in this way for starting materials and run products along with 95% confidence limits.

RESULTS

BSE images in Figures 3 and 4 illustrate significant changes in texture with time, including changes in size of zircon and quartz crystals and pores. Zircon crystals are spherical or nearly so, with mean measured shape factors ranging from ~0.8 to 0.95 (Table 1; a perfect sphere has a shape factor of one). Here we report zircon crystal size in terms of Feret diameter D in micrometers because it is more familiar and more easily measured than mean intercept length L (see discussion in Ayers et al. 1999). However, mean values $\langle D \rangle$ and $\langle L \rangle$ reported in Table 1 are very similar, and the distribution of measured values for a given sample is nearly identical (cf., Figs. 2c and 2e). As observed by Ayers et al. (1999) in a parallel study of monazite growth in quartzite at the same conditions, fluid wetting angles in run products are typically >60°, indicating that fluid is non-wetting. However, as shown below, the presence of fluid greatly increases the rate of textural development.

QUARTZ GROWTH

Although we did not measure quartz crystal size, we observed qualitatively that quartz crystals grow with time (cf., Figs. 3 and 4). Quartz growth was unimpeded by the presence of zircon crystals on quartz-quartz grain boundaries, suggesting that zircon crystals were not large enough to "pin" quartz grain boundaries (Watson et al. 1989). Zircon crystals must have maintained their energetically favorable positions on moving quartz grain boundaries by dissolving in and precipitating from the fluid. Fluid-mediated recrystallization (simultaneous dissolution and precipitation with or without transport of dissolved material) and growth of zircon and quartz drives the system toward textural equilibrium and the lowest possible Gibbs free energy. Under fluid-absent conditions, we qualitatively observed no significant growth of quartz after 72 h, similar to the observations of Tullis and Yund (1982).

Zircon growth

In the oxide-series experiments containing H_2O, ZrO_2 in the starting material reacted with quartz to form zircon very rapidly. Unreacted ZrO_2 was not found in the run products of the zero time experiment (ZG no. 24, Fig. 2c), suggesting that the reaction $ZrO_2 + SiO_2 = ZrSiO_4$ went to completion during the 20 min of heating from room temperature to 1000 °C. The CSFH of this freshly nucleated zircon is lognormal as expected (Figs. 2c–2e). In contrast, a 24 h anhydrous experiment (ZG no. 9) did not produce zircon, suggesting that fluid is required for the zircon-forming reaction. In the run products of hydrous experiments of longer duration, ZrO_2 identified using energy dispersive spectrometry accounted for <<1 wt% of Zr-bearing crystals, where it occurred as relatively large clots of unreacted powder. Comparison of oxide-series run products for t = 0 h (ZG no. 24, Fig. 2c) and t = 336 h (ZG no. 20, Fig. 3d) shows that textural changes are dominated by coarsening of quartz and pores.

Results of a series of hydrous experiments performed using the oxide starting material (Fig. 3) show that, at t = 0 (ZG no. 24), mean zircon diameter $\langle D \rangle = 0.59 \pm 0.04$ μm, which after 22.2 h (ZG no. 23) decreased to 0.52 ± 0.02 μm. Zircon then increased in size with increasing experiment duration to 1.20 ± 0.04 μm after 336 h (ZG no. 20). These results can be reconciled with results reported in Ayers et al. (1996) if the sample labels on ZG no. 6 and ZG no. 10 reported in that study are switched. To determine the form of the growth equation log ($\langle D \rangle^n - \langle D_0 \rangle^n$) was plotted vs. log ($t - t_0$) for values of n = 2, 3, and 4, where $\langle D_0 \rangle$ is the mean diameter for the shortest experiment of duration t_0 in the series. For both sets of data a value of n = 2 provided the best fit to the data (Fig. 6).

Zircon crystal size in the "silicate" starting material containing $ZrSiO_4$ was characterized two ways. Powder was mounted in epoxy, polished, and imaged, yielding $\langle D \rangle = 0.53 \pm 0.05$ μm ("ZG SM" in Table 1). A time-zero experiment (ZG no. 26) yielded $\langle D \rangle = 0.63 \pm 0.04$ μm (Fig. 2b). As observed in the run products of the oxide-series experiments, $\langle D \rangle$ decreased, to a value of 0.32 ± 0.02 μm at t = 8 h (ZG no. 12) (Fig. 4a). This behavior, also observed for monazite in similar experiments (Ayers et al. 1999), suggests that zircon either progressively dissolved or recrystallized in the first 8 h. Based on the very low aqueous solubility of monazite at these conditions (Ayers and Watson 1991), Ayers and others (1999) concluded that the initial decrease in crystal size resulted from recrystallization, possibly due to the presence of crystals strained during grinding. Thus, the initial decrease in size is an artifact arising from methods used for sample preparation and is not representative of any natural process.

After 8 h, zircon began to coarsen (Fig. 7), reaching a mean diameter of 0.80 ± 0.02 μm after t = 133.4 h (ZG no. 18, Fig. 4d). Run products from the longest duration hydrous experiment show evidence of significant growth of quartz and of pore

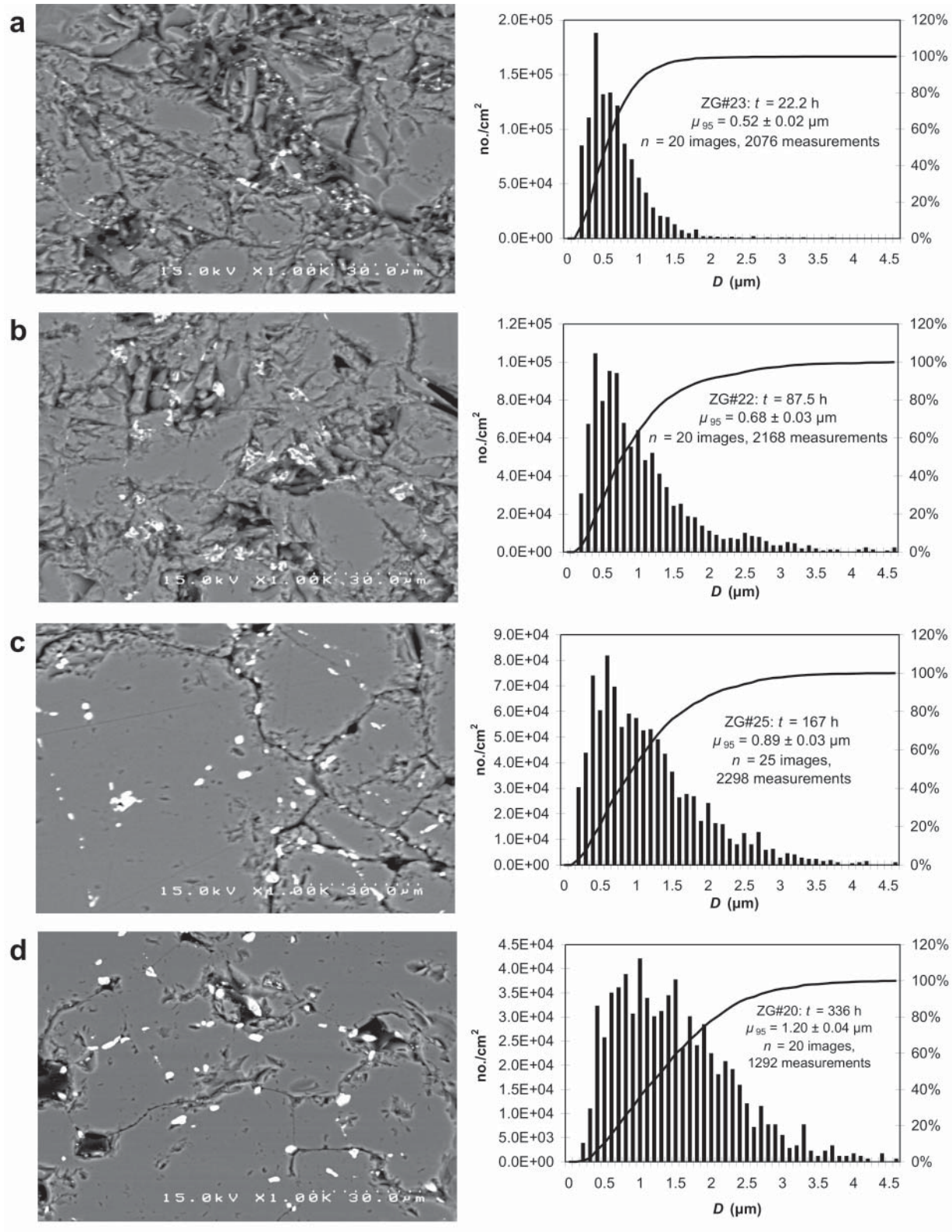

FIGURE 3. BSE images and CSFH of run products from experiments containing H_2O and oxide starting material. In these and all subsequent CSFH, the solid curve is the measured cumulative frequency in percent.

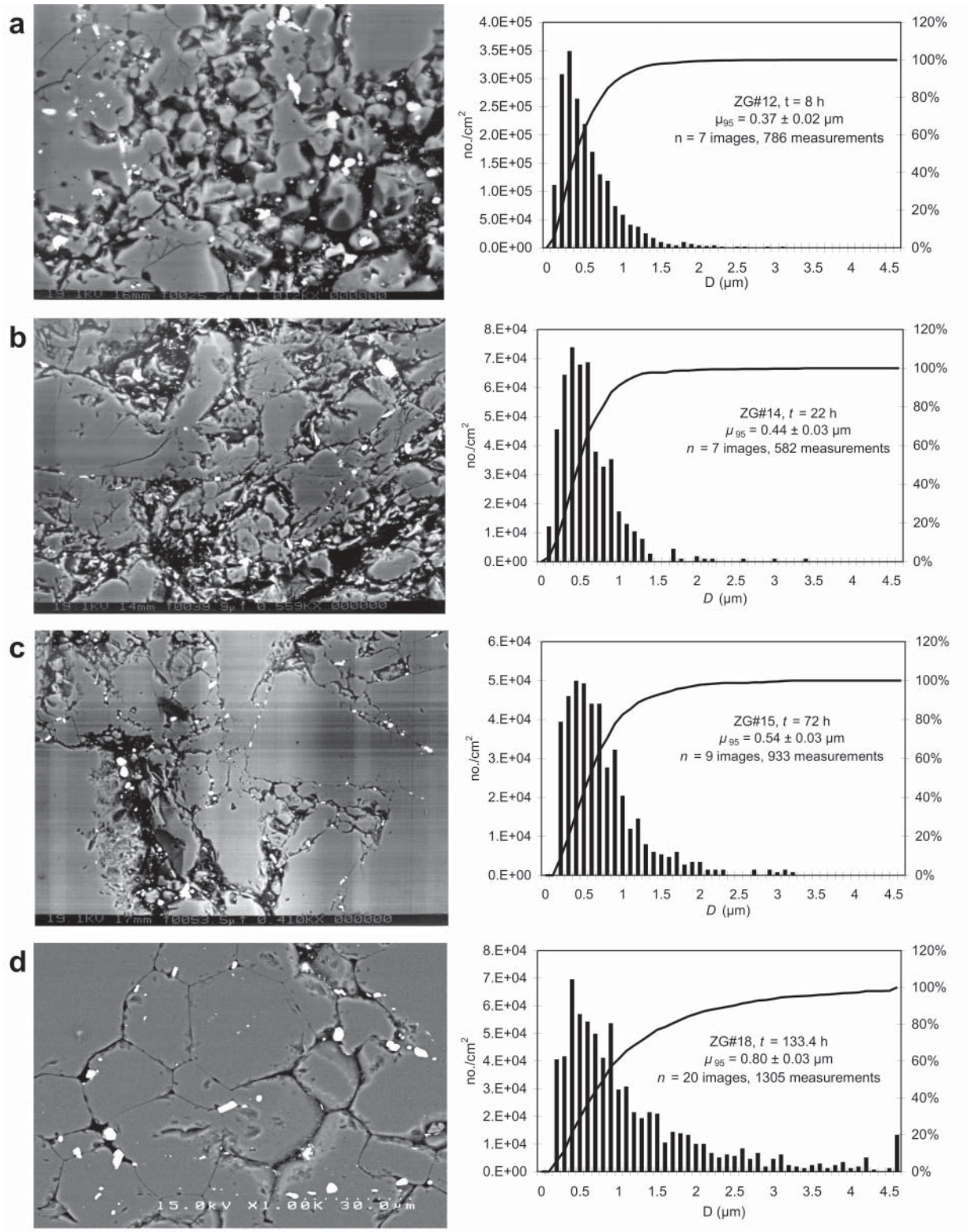

FIGURE 4. BSE images and CSFH of run products from experiments containing H_2O and silicate starting material.

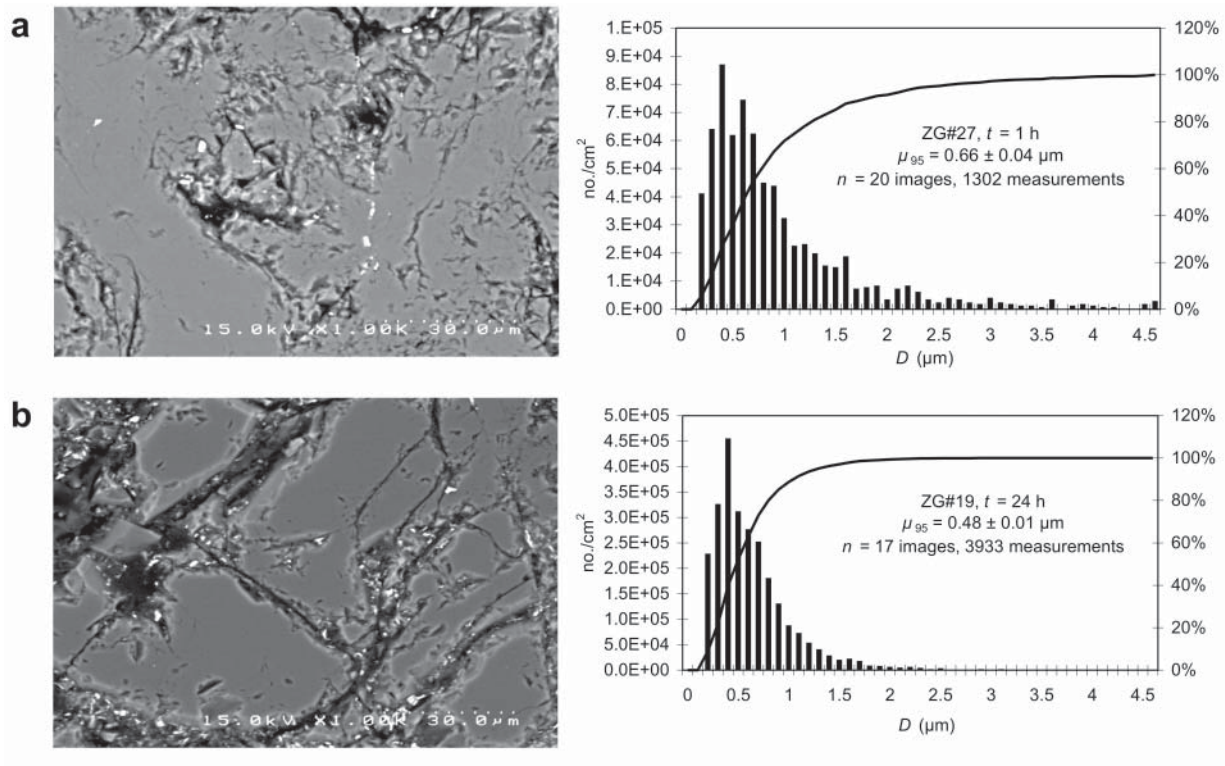

FIGURE 5. BSE images and CSFH of run products from anhydrous experiments with silicate starting material.

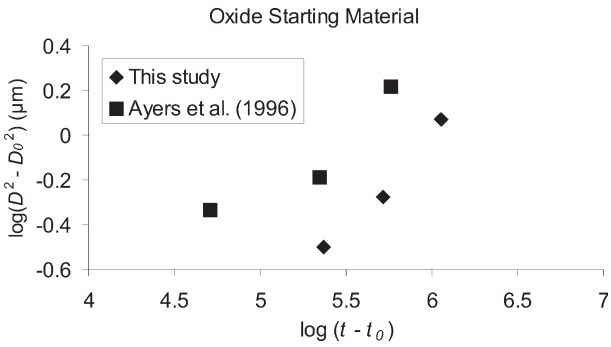

FIGURE 6. Results from experiments with oxide starting material. D_0 is the mean diameter of zircon in the run products of the shortest duration experiment.

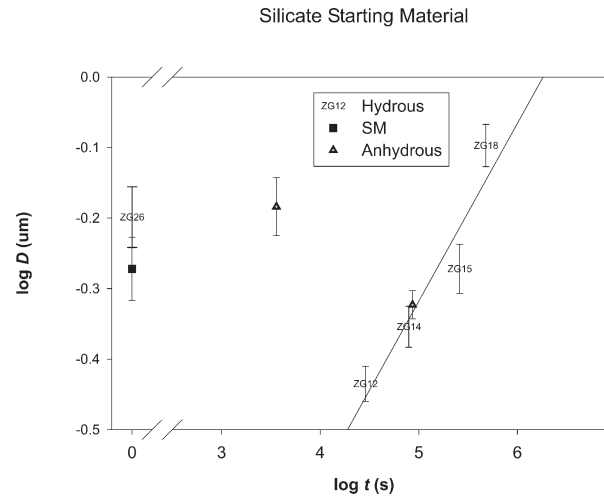

FIGURE 7. Summary of results for silicate starting material. Results from experiments containing ~1 wt% H_2O ("Hydrous") labeled with experiment number. "SM" is starting material mounted as powder in epoxy for measurement. The zero-time experiment yielded a similar value of mean diameter.

size, while zircon occurs almost exclusively on grain boundaries and usually near pores (Fig. 4d). Zircons on grain boundaries appear significantly larger than those trapped as inclusions.

Run products from anhydrous experiments on silicate starting material show angular quartz fragments with unhealed cracks similar to those in the starting material, even after 24 h (Fig. 5). We infer that fluid significantly enhances rates of coarsening and textural development. Zircon crystal size did not change significantly between t = 0 h (ZG no. 26) when $\langle D \rangle$ = 0.63 ± 0.04 µm (Fig. 2) and t = 1 h (ZG no. 27) when $\langle D \rangle$ = 0.66 ± 0.04 µm (Fig. 5a). At t = 24 h (ZG no. 19) $\langle D \rangle$ had decreased to 0.48 ± 0.01 µm (Fig. 5b). We conclude that no significant growth occurred in our anhydrous experiments, although it is unclear from the three experiments how zircon crystal size depends on time (Fig. 7).

Combining results from hydrous experiments on oxide and silicate starting materials [neglecting the results on oxide starting material reported by Ayers et al. (1996) and the 72 h experiments] yields a straight line with a remarkably good fit (Fig. 8): $\log (\langle D\rangle^n - \langle D_0\rangle^n) = \log (\langle D\rangle^2 - \langle D_0\rangle^2) = \log (t - t_0) + \log K_n = \log (t - t_0) - 5.9$, where $\langle D\rangle$ is the mean diameter in μm, the subscript 0 denotes initial value at time zero, t is experiment duration in seconds, and K_n is the growth rate constant with units of μm²/s (five experiments, $r^2 = 0.988$). A value of $n = 2$ suggests that growth is interface controlled, with the rate limited by dissolution and precipitation on the crystal surface. Thus, the growth rate equation that best describes our data is $\langle D\rangle - \langle D_0\rangle = K_{1/n}\, t^{1/n} = K_n^{1/n}\, t^{1/n} = (1.12 \times 10^{-3}\ \mu m/s^{1/2}) t^{1/2}$, a parabolic rate law.

DISCUSSION

Our experiments were designed so that zircon could grow only by Ostwald ripening, i.e., coarsening of a dispersed phase. We found that zircon coarsens at a measurable rate at 1.0 GPa and 1000 °C. The driving force is the same as that for the observed coarsening of matrix quartz: small crystals are more soluble in the fluid than large crystals, producing concentration gradients in pore fluid that lead to diffusion of dissolved components from small to large crystals. It is widely accepted that quartz in quartzites and calcite in marbles coarsen during prolonged annealing of natural rocks (Joesten 1991). The driving force is minimization of surface free energy, the same driving force as for coarsening of dispersed phases such as zircon during metamorphism. Many rocks do not contain minerals other than zircon that contain significant concentrations of Zr. For such rocks, the only potential growth mechanism for zircon is coarsening.

Intracrystalline zoning and recrystallization

Zircon crystals in our run products show no evidence of internal zoning. This may result from several factors, including (1) zircon in our starting material was chemically homogeneous (unzoned); (2) the crystals are too small for zoning to develop or be imaged using cathodoluminescence (CL) or backscattered electrons; and (3) recrystallization homogenized the compositions of the zircon crystals. The crystals were not homogenized by intracrystalline diffusion because, even at experimental conditions of 1000 °C, the diffusivities of CL active ions such as REE are only ~10^{-25} m²/s (Cherniak et al. 1997), resulting in diffusion half-lengths of only 7×10^{-4} μm even for the longest experiment of t = 336 h.

Recrystallization of zircon during coarsening results from small crystals dissolving and large crystals growing. Recrystallization driven by Ostwald ripening alone does not change the positions of crystals, only their sizes. Zircon also recrystallizes in response to coarsening of the quartz matrix: zircon crystals migrate with and maintain their energetically favorable positions on moving quartz grain boundaries, changing their positions but not necessarily their sizes. The overall rate of recrystallization should equal the sum of the amounts attributable to Ostwald ripening and matrix coarsening-induced grain migration, and should increase with increasing rate of matrix coarsening. In both cases recrystallization is accomplished through dissolution/precipitation in the fluid (as evidenced by our obtained value of n = 2, and the lack of recrystallization in anhydrous experiments). We conclude that fluid-assisted recrystallization produced the unzoned crystals observed in our run products.

Natural zoned zircon crystals may preserve their zoning during matrix coarsening if they are large enough to pin grain boundaries or if they are trapped as inclusions. In contrast, small zircon crystals that recrystallize and move with mobile grain boundaries will homogenize, as happened in our experiments. Natural zircons collected to date show no convincing evidence of the elimination of internal zoning by matrix coarsening. In part, this may result from collection of samples biased toward large crystals that may have pinned grain boundaries, or it may be that most or all of the observed zircons were present as inclusions.

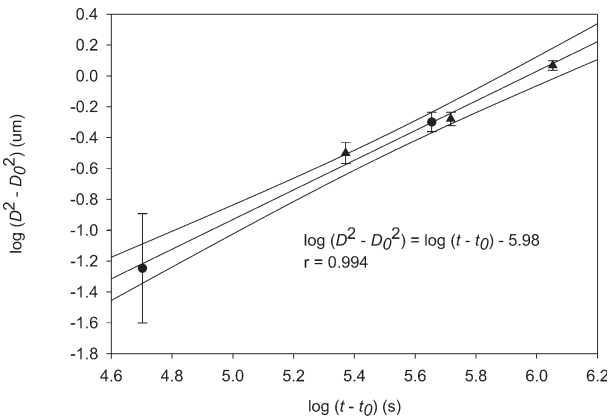

FIGURE 8. Plot of combined results from experiments using oxide (ZrO_2, diamonds) and silicate ($ZrSiO_4$, circles) starting material. Units are D (μm) and t (s). From propagation of errors the standards deviation $s = \frac{0.434\sqrt{2\left(D \cdot S_D + D_0 \cdot S_{D_0}\right)}}{D^2 - D_0^2}$ and 95% C.L. (plotted) = $\frac{1.96s}{\sqrt{n}}$.

Growth rate equation

According to LSW theory (Joesten 1991), n should be an integer with the following possible values corresponding to rate-limiting factors: 2 (interface-controlled reaction kinetics), 3 (growth rate limited by volume diffusion), or 4 (growth rate limited by grain boundary diffusion). The best fit is provided by n = 2 (Fig. 8), suggesting that the rate of Ostwald ripening of zircon is limited by the rate of dissolution or precipitation on the crystal surface. In this situation, the concentration of dissolved zircon in the fluid is the same everywhere because the rate of diffusion in the intergranular fluid is greater than the rates of dissolution and precipitation. The fluid is undersaturated with respect to crystals with radii less than the critical radius and oversaturated in crystals with $r > r^*$, where r^* is the critical radius below which crystals dissolve and above which crystals grow; it is equal to the mean radius for n = 3 and 8/9 of the mean radius for n = 2 (Rahaman 1995).

Figure 9 compares the measured CSFH of zircon in the run products of the shortest (ZG no. 24, t = 0 h) and longest (ZG no. 20, t = 336 h) experiments with the steady-state profiles

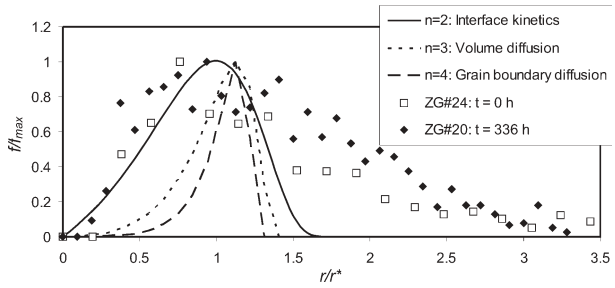

FIGURE 9. Comparison of observed and theoretical CSFH. On the y-axis, the frequency (probability) is normalized so that the peak value = 1. On the x-axis, crystal size is normalized by dividing radius by the critical radius r^*, defined as the radius below which crystals dissolve and above which crystals grow.

predicted by LSW theory for values of $n = 2$, 3, and 4. There is a slight change in shape of the zircon CSFH with time, particularly an increase in the normalized frequency of crystals with values r/r^* between 1 and 2. Furthermore, the broad distribution of measured sizes and the peak in the distribution at $r/r^* < 1$ is most consistent with the LSW distribution for $n = 2$. The longest experiment is closer to the theoretical equilibrium distribution than is the shortest experiment, suggesting that the observed coarsening is moving the system toward textural equilibrium. However, even after 336 h, the observed CSFH is far from conforming to the theoretical equilibrium CSFH for $n = 2$, consistent with the conclusion based on results of numerical modeling that the approach to a steady-state profile is slow and may never be reached (Eberl et al. 1998). Further evidence that Ostwald ripening has barely begun in our experiments is that the variance of measured diameters (Table 1) does not decrease with time as it should. We conclude that significant coarsening may occur before an equilibrium CSFH is achieved, and therefore measurement of CSFH in natural rocks may not always accurately indicate the growth mechanism.

The growth rate equation obtained by combining results from the oxide and silicate series can be used to estimate the amount of time required to grow a zircon crystal or a rim of specified size (Fig. 10). At 1000 °C, $D - D_0 = K_{1/n}t^{1/n} = (1.12 \times 10^{-3}\ \mu m/s^{1/2})\ t^{1/2}$. For a 5 μm thick rim grown over a 10 μm diameter core, $D = 20$ μm and $D - D_0 = 10$ μm, so that t (s) = $(10\ \mu m/1.12 \times 10^{-3}\ \mu m/s^{0.5})^2 = 7.9 \times 10^7$ s = 2.5 years. Thus, coarsening of zircon is relatively rapid at 1000 °C in the presence of aqueous fluid.

Growth by coalescence

In our parallel study of monazite growth (Ayers et al. 1999), we commonly found crystals that appeared to be coalescing to form a single crystal from two or more other ones, as evidenced by a crystal outline that "pinched out" near the center to produce a dumbbell-shaped crystal, sometimes with a visible grain boundary bisecting the crystal. Coalescence may occur when grains are close together, such as may occur when matrix coarsening causes zircons to migrate with moving grain boundaries (imagine a small quartz grain being consumed and the zircons on its grain boundaries being pushed together). Although not as common in the run products of the zircon growth experiments, coalescence was observed in many cases, and coalescing crystals can be found in Figures 3 and 4.

Coalescence (agglomeration) of zircon crystals during matrix coarsening may temporarily produce crystals with composite zoning. In Figure 11, a zircon from the Winding Stair Gap granulite-facies metapelite (Miller et al. 1998) exhibits the characteristic pinched-out outline. With time, the boundary between the two grains should migrate through the smaller one, erasing its internal zoning. This is because when two crystals of unlike size come together, they are likely to be in different crystallographic orientations, and the grain boundary separating the two crystals is the interface between two mismatched crystal lattices. The surface of the smaller crystal is more

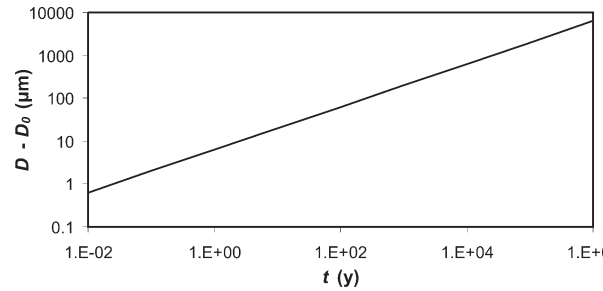

FIGURE 10. Plot of $D - D_0$ (μm) vs. time (y) calculated from $D - D_0 = K_{1/n}t^{1/n} = (1.12 \times 10^{-3}\ \mu m/s^{1/2})\ t^{1/2}$. The y-axis represents the diameter of a newly grown zircon crystal ($D_0 = 0$), or twice the thickness of a rim formed on an older core by coarsening.

FIGURE 11. Natural zircon crystal with composite Grenville age cores and Ordovician age rims. From Winding Stair Gap granulite grade metapelite, southern Appalachian Blue Ridge (Miller et al. 1998).

strongly curved and therefore of higher energy than the surface of the larger crystal. Accordingly, atoms preferentially detach from the surface of the smaller crystal and reorient themselves to align with the lattice of the larger crystal to which they attach. This process of dissolution of the smaller crystal and precipitation onto the larger crystal causes the grain boundary to migrate through the smaller crystal, inducing complete recrystallization and loss of internal zoning (Rahaman 1995). It is the same process that affects host crystals during matrix coarsening, and corresponds to normal grain growth (n = 2) limited by surface kinetics. If coalescence were the primary growth mechanism for zircon in our experiments, we would expect that our experimental data in Figure 8 would be best fit with an exponent n = 2. That it does suggests that coalescence may be an important growth mechanism in our experiments. However, although coalescence may occur simultaneously with ripening, it may be difficult to identify in natural rocks because it does not necessarily affect the shape of the CSFH (Eberl et al. 1998).

Growth during anatexis

An alternative explanation for zircon overgrowths is that they form during anatexis. Melt may play the same role as fluid by acting as a fast-diffusion pathway, thereby enhancing zircon growth rate. In the polythermal model, temperature in a closed system increases and zircons dissolve in the melt until the melt becomes saturated. Subsequent cooling and reprecipitation leads to formation of overgrowths with U-Pb ages that record the timing of anatexis (Watson 1996). However, the mass of overgrowths in some rocks exceeds the amount that could be dissolved in anatectic melt at the appropriate temperature and melt composition (Nemchin and Pidgeon 2001). These overgrowths may have formed isothermally by Ostwald ripening in the presence of zircon-saturated melt. Vavra et al. (1999) invoked this mechanism to explain their observation of zircons in restites from quartzofeldspathic metasediments with rounded, thick, nebulously zoned, high CL rims mantling low CL cores with oscillatory zoning. Anatexis began in the upper-amphibolite facies, and zircon growth accelerated as prograde metamorphism progressed to the granulite facies. In many cases, the volume of zircon rims exceeded that in the cores, ruling out a simple batch dissolution/reprecipitation growth mechanism. Thus, Ostwald ripening may be an important growth mechanism when either fluid or melt is present.

Implications for isotopic dating

Recrystallization of zircon induced by matrix coarsening should erase preexisting internal zoning and reset isotopic clocks. Fluid-bearing rocks that have experienced prolonged high-temperature metamorphism should contain completely recrystallized, unzoned zircon crystals on grain boundaries. These crystals should yield U-Pb ages corresponding to the timing of thermal metamorphism. Some zircon crystals may grow large enough to pin grain boundaries, in which case, preexisting cores will be preserved and be mantled by metamorphic rims. Zircons above the critical radius for Ostwald ripening (but not large enough to pin grain boundaries) may become occluded in growing matrix crystals. Zircon inclusions in large matrix crystals may be unaffected by matrix coarsening, and so preserve age information for events predating thermal metamorphism. The preservation of old ages by "shielded" accessory minerals was predicted for monazite by Ayers et al. (1999) and recently confirmed for monazite in Hercynian kinzigites by Montel et al. (2000).

Growth of zircon by Ostwald ripening is rapid at 1000 °C in the presence of fluid. The rapid rate of zircon coarsening may explain why ages measured across overgrowths are indistinguishable (Nemchin and Pidgeon 2001). The presence of fluid greatly increases the rate of coarsening of zircon. Fluid influx may cause zircon to grow in a rapid burst, i.e., zircon growth is nearly instantaneous in terms of geologic time. Melt may have the same effect as fluid by acting as a fast diffusion pathway. Thus, measured ages of metamorphic overgrowths may correspond to the timing of fluid influx, or anatexis.

ACKNOWLEDGMENTS

This research was made possible by NSF grant EAR-9506551 to Miller and Ayers and a Vanderbilt University Summer Research scholarship to DeLaCruz. Thanks to the Smithsonian National Museum of Natural History for providing the natural zircon used in the starting materials. Thanks also to Raymond Joesten and Gerhard Vavra for very detailed and helpful reviews.

REFERENCES CITED

Ayers, J.C. and Watson, E.B. (1991) Solubility of apatite, monazite, zircon and rutile in supercritical aqueous fluids with implications for subduction zone geochemistry. Philosophical Transactions Royal Society London A, 335, 365–375.

Ayers, J.C., Brenan, J.B., Watson, E.B., Wark, D.A., and Minarik, W.G. (1992) A new capsule technique for hydrothermal experiments using the piston cylinder apparatus. American Mineralogist, 77, 1080–1086.

Ayers, J.C., de la Cruz, K.J., Gorisch, E.B., and Miller, C.F. (1996) Experimental measurement of the growth rate of zircon; an assessment of the importance of Ostwald ripening during high-grade metamorphism, with implications for U-Pb chronology. Abstracts with Programs, 28, p. 357. Geological Society of America, Denver, Colorado.

Ayers, J.C., Miller, C., Gorisch, B., and Milleman, J. (1999) Textural development of monazite during high-grade metamorphism; hydrothermal growth kinetics, with implications for U, Th-Pb geochronology. American Mineralogist, 84, 1766–1780.

Ayers, J.C., Dunkle, S., Gao, S., and Miller, C. (2002) Triassic zircon U-Pb and monazite Th-Pb ages recorded in Maowu ultramafics and Shuanghe jadeite quartzite, Dabie Shan UHP belt, east-central China. Chemical Geology, 186, 315–331.

Cashman, K.V. and Ferry, J.M. (1988) Crystal size distribution (CSD) in rocks and the kinetics and dynamics of crystallization III. Metamorphic crystallization. Contributions to Mineralogy and Petrology, 99, 401–415.

Cherniak, D.J. and Watson, E.B. (2000) Pb diffusion in zircon. Chemical Geology, 172, 5–24.

Cherniak, D.J., Hanchar, J.M., and Watson, E.B. (1997) Rare-earth diffusion in zircon. Chemical Geology, 134, 289–301.

Eberl, D.D. (1998) Deducing growth mechanisms for minerals from the shapes of crystal size distributions. American Journal of Science, 298, 499–533.

Fraser, G., Ellis, D., and Eggins, S. (1997) Zirconium abundance in granulite-facies minerals, with implications for zircon geochronology in high-grade rocks. Geology, 25, 607–610.

Geisler, T. and Schleicher, H. (2000) Improved U-Th-total Pb dating of zircons by electron microprobe using a simple new background modeling procedure and Ca as a chemical criterion of fluid-induced U-Th-Pb discordance in zircon. Chemical Geology, 163, 269.

Hanchar, J.M. and Miller, C.F. (1993) Zircon zonation patterns as revealed by cathodoluminescence and backscattered secondary electron images: Implications for interpretation of complex crustal histories. Chemical Geology, 110, 1–13.

Horn, I., Rudnick, R.L., and McDonough, W.F. (2000) Precise elemental and isotope ratio determination by simultaneous solution nebulization and laser ablation-ICP-MS: application to U-Pb. Chemical Geology, 164, 281.

Joesten, R.L. (1991) Kinetics of coarsening and diffusion-controlled mineral growth. In D.M. Kerrick, Ed., Contact metamorphism, 26, p. 507–582. Reviews in Mineralogy, Mineralogical Society of America, Washington, D.C.

Kingsbury, J.A., Miller, C.F., Wooden, J.L., and Harrison, T.M. (1993) Monazite paragenesis and U-Pb systematics in rocks of the eastern Mojave Desert, California: Implications for thermochronometry. Chemical Geology, 110, 147–168.

Lasaga, A.C. (1998) Kinetic theory in the earth sciences. 811 p. Princeton University Press, Princeton, New Jersey.

Liati, A. and Gebauer, D. (1999) Constraining the prograde and retrograde P-T-t path of Eocene HP rocks by SHRIMP dating of different zircon domains: inferred rates of heating, burial, cooling and exhumation for central Rhodope, northern Greece. Contributions to Mineralogy and Petrology, 135, 340.

Machado, N. and Gauthier, G. (1996) Determination of 207Pb/206Pb ages on zircon and monazite by laser-ablation ICPMS and application to study of sedimentary provenance and metamorphism in southeastern Brazil. Geochimica et Cosmochimica Acta, 60, 5063–5074.

Miller, C.F., Hatcher, R.D.J., Harrison, T.M., Coath, C.D., and Gorisch, E.B. (1998) Cryptic crustal events elucidated through zone imaging and ion microprobe studies, southern Appalachian Blue Ridge, North Carolina-Georgia. Geology, 26, 419–422.

Miller, C.F., Hatcher, R.D., Jr., Ayers, J.C., Coath, C.D., and Harrison, T.M. (2000) Age and zircon inheritance of eastern Blue Ridge plutons, southwestern North Carolina and northeastern Georgia, with implications for magma history and evolution of the Southern Appalachian Orogen. American Journal of Science, 300, 142–172.

Montel, J.M., Kornprobst, J., and Vielzeuf, D. (2000) Preservation of old U-Th-Pb ages in shielded monazite; example from the Benmi Bousera Hercynian kinzigites (Morocco). Journal of Metamorphic Geology, 18, 335–342.

Nemchin, A.A. and Pidgeon, R.T. (2001) Problems in the Interpretation of the Origin of Zircon Overgrowths. Eleventh Annual Goldschmidt Conference, Abstract no. 3529. LPI Contribution No. 1088, Lunar and Planetary Institute, Houston (CDROM).

Pidgeon, R.T., Macambira, M.J.B., and Lafon, J.M. (2000) Th-U-Pb isotopic systems and internal structures of complex zircons from an enderbite from the Pium Complex, Carajas Province, Brazil: evidence for the ages of granulite facies metamorphism and the protolith of the enderbite. Chemical Geology, 166, 159.

Rahaman, M.N. (1995) Ceramic processing and sintering. 770 p. M. Dekker, New York.

Roberts, M.P. and Finger, F. (1997) Do U-Pb zircon ages from granulites reflect peak metamorphic conditions? Geology, 25, 319–322.

Rubatto, D., Williams, I.S., and Buick, I.S. (2001) Zircon and monazite response to prograde metamorphism in the Reynolds Range, central Australia. Contributions to Mineralogy and Petrology, 140, 458.

Russ, J.C. (1990) Computer-assisted microscopy. Plenum Press, New York.

Sorensen, S.S. and Grossman, J.N. (1989) Enrichments of trace elements in garnet amphibolites from a paleo-subduction zone: Catalina Schist, southern California. Geochimica et Cosmochimica Acta, 53, 3155–3178.

Tullis, J. and Yund, R.A. (1982) Grain growth kinetics of quartz and calcite aggregates. Journal Geology, 90, 301–318.

Vavra, G., Gebauer, D., Schmid, R., and Compston, W. (1996) Multiple zircon growth and recrystallization during polyphase Late Carboniferous to Triassic metamorphism in granulites of the Ivrea Zone (Southern Alps); an ion microprobe (SHRIMP) study. Contributions to Mineralogy and Petrology, 122, 337–358.

Vavra, G., Schmid, R., and Gebauer, D. (1999) Internal morphology, habit and U-Th-Pb microanalysis of amphibolite-to-granulite facies zircons: geochronology of the Ivrea Zone (Southern Alps). Contributions to Mineralogy and Petrology, 134, 380–404.

Watson, E.B. (1996) Dissolution, growth and survival of zircons during crustal fusion: kinetic principles, geological models and implications for isotopic inheritance. Transactions Royal Society Edinburgh: Earth Sciences, 87, 43–56.

Watson, E.B., Vicenzi, E.P., and Rapp, R.P. (1989) Inclusion/host relations involving accessory minerals in high-grade metamorphic and anatectic rocks. Contributions to Mineralogy and Petrology, 101, 220–231.

MANUSCRIPT RECEIVED NOVEMBER 6, 2001
MANUSCRIPT ACCEPTED OCTOBER 11, 2002
MANUSCRIPT HANDLED BY ROBERT J. TRACY